

# Molecular Superbubbles and Outflows from the Starburst Galaxy NGC 2146

An-Li TSAI,<sup>1,2</sup> Satoki MATSUSHITA,<sup>2</sup> Kouichiro NAKANISHI,<sup>3</sup> Kotaro KOHNO,<sup>4</sup>  
Ryohei KAWABE,<sup>3</sup> Tatsuya INUI,<sup>5</sup> Hironori MATSUMOTO,<sup>5</sup>  
Takeshi G. TSURU,<sup>5</sup> Alison B. PECK,<sup>6</sup>

and

Andrea TARCHI,<sup>7,8</sup>

<sup>1</sup>*Department of Earth Sciences, National Taiwan Normal University,*

*No.88, Dingzhou Rd. Sec. 4, Taipei 11677, Taiwan*

*altsai@asiaa.sinica.edu.tw*

<sup>2</sup>*Academia Sinica, Institute of Astronomy and Astrophysics, P.O. Box 23-141, Taipei 10617, Taiwan*

<sup>3</sup>*Nobeyama Radio Observatory, Minamimaki, Minamisaku, Nagano 384-1305*

<sup>4</sup>*Institute of Astronomy, University of Tokyo, 2-21-1 Osawa, Mitaka, Tokyo 181-0015*

<sup>5</sup>*Department of Physics, Faculty of Science, Kyoto University, Sakyo-ku, Kyoto 606-8502*

<sup>6</sup>*Joint ALMA Office, Av El Golf 40, Piso 18, Santiago, Chile*

<sup>7</sup>*INAF - Osservatorio Astronomico di Cagliari, Loc. Poggio dei Pini, Strada 54, 09012 Capoterra, Italy*

<sup>8</sup>*INAF - Istituto di Radioastronomia, via Gobetti 101, 40129 Bologna, Italy*

(Received 2008 December 15; accepted 2009 April 25)

## Abstract

We present results from a deep ( $1\sigma = 5.7$  mJy beam<sup>-1</sup> per 20.8 km s<sup>-1</sup> velocity channel) <sup>12</sup>CO(1-0) interferometric observation of the central 60'' region of the nearby edge-on starburst galaxy NGC 2146 observed with the Nobeyama Millimeter Array (NMA). Two diffuse expanding molecular superbubbles and one molecular outflow are successfully detected. One molecular superbubble, with a size of  $\sim 1$  kpc and an expansion velocity of  $\sim 50$  km s<sup>-1</sup>, is located below the galactic disk; a second molecular superbubble, this time with a size of  $\sim 700$  pc and an expansion velocity of  $\sim 35$  km s<sup>-1</sup>, is also seen in the position-velocity diagram; the molecular outflow is located above the galactic disk with an extent  $\sim 2$  kpc, expanding with a velocity of up to  $\sim 200$  km s<sup>-1</sup>. The molecular outflow has an arc-like structure, and is located at the front edge of the soft X-ray outflow. In addition, the kinetic energy ( $\sim 3 \times 10^{55}$  erg) and the pressure ( $\sim 1 \times 10^{-12\pm 1}$  dyne cm<sup>-2</sup>) of the molecular outflow is comparable to or smaller than that of the hot thermal plasma, suggesting that the hot plasma pushes the molecular gas out from the galactic disk. Inside the  $\sim 1$  kpc size molecular superbubble, diffuse soft X-ray emission seems to exist. But since the superbubble

lies behind the inclined galactic disk, it is largely absorbed by the molecular gas.

**Key words:** ISM: bubbles — ISM: jets and outflows — galaxies: individual (NGC 2146) — galaxies: ISM — galaxies: starburst

## 1. Introduction

A starburst galaxy is characterized by strong star forming activity. Starburst phenomena usually occur in the central regions of galaxies, and produce large numbers of massive stars on short time scales with star formation rates tens or hundreds of times higher than those in normal galaxies. Through stellar winds and energetic supernova explosions, these massive stars generate a large amount of mechanical energy that can sweep the surrounding interstellar medium (ISM) from starburst regions, create ISM bubbles, and generate high velocity galactic winds. This hypothetical starburst evolution is supported by several numerical models (e.g., Tomisaka & Ikeuchi 1988; Strickland & Stevens 2000; Marcolini et al. 2005), and is actually based on various observational results. Shell-like structures and outflows have been observed in many starburst galaxies in optical emission lines and soft X-ray emission (e.g., Lehnert & Heckman 1996; Martin 1998; Dahlem et al. 1998; Strickland et al. 2004). Shell-like structures are also often observed in nearby galaxies in the atomic hydrogen (HI) line (e.g., Tenorio-Tagle & Bodenheimer 1988).

Evidence for these shell-like or outflowing features from starburst galaxies are, however, rarely seen using molecular tracers. The famous cases are the molecular outflows in M82 (Nakai et al. 1987) and NGC 891 (Handa et al. 1992), and molecular bubbles in NGC 3628 (Irwin & Sofue 1996). The reasons for the rarity of such detections are mostly their diffuse and extended nature and the lack of sensitive detections in this wavelength range. Recent improvements of various instruments at millimeter-wave have resulted in progress in this field: The interferometric  $^{12}\text{CO}(1-0)$  observations toward M82 succeeded in imaging molecular superbubbles and outflows (e.g., Neininger et al. 1998; Weiss et al. 1999; Matsushita et al. 2000; Weiss et al. 2001), and revealed a self-induced starburst mechanism (Matsushita et al. 2005). Molecular superbubbles and/or outflows have also been detected in NGC 253 (Sakamoto et al. 2006), NGC 4631 (Rand 2000), and NGC 4666 (Walter et al. 2004). Since stars form from molecular gas, observing these peculiar features in molecular gas can provide information about the regulation and feedback processes of the starburst phenomena. Here we report a new example of molecular superbubbles and outflows from the starburst galaxy NGC 2146.

NGC 2146 is a nearby (17.2 Mpc,  $1'' = 80$  pc; Tully 1988), IR luminous ( $1.2 \times 10^{11} L_{\odot}$ ; Sanders et al. 2003), edge-on ( $i = 63^{\circ}$ ; Della Ceca et al. 1999) starburst galaxy. Its optical appearance shows disturbed features with peculiar spiral arms, which cannot be explained by a simple model of spiral structure (Benvenuti et al. 1975; Greve et al. 2006). The neutral hydrogen

images display 100 kpc scale tidal tails, although there is no evidence of a nearby companion galaxy (Fisher & Tully 1976; Taramopoulos et al. 2001). A large amount of molecular gas is concentrated around the central region, which is enough to support the starburst activities (Jackson & Ho 1988; Young et al. 1988). The central region hosts several compact radio continuum sources, identified as supernova remnants, radio supernovae, and ultra-compact and/or ultra-dense HII regions (Tarchi et al. 2000). The soft X-ray images show kpc-scale outflows from the starburst region around the galactic center (Inui et al. 2005; Della Ceca et al. 1999; Armus et al. 1995). All these characteristics are reminiscent of those present in the nearby starburst galaxy M82, where kpc-scale outflows have also been detected, together with a molecular superbubble. Given the similarity between the two galaxies, it is natural to expect that similar features can be revealed also in NGC 2146. Therefore, we have performed deep observations in the  $^{12}\text{CO}(1-0)$  line toward the central region of NGC 2146 as a case study for molecular superbubbles and outflows.

## 2. Observations and Data Reductions

We performed deep  $^{12}\text{CO}(1-0)$  observations toward the central  $60''$  region of the edge-on starburst galaxy NGC 2146 with the Nobeyama Millimeter Array (NMA), which consists of six 10-meter antennas located at the Nobeyama Radio Observatory (NRO). The observations were made during 2001 November to 2002 April with three configurations. The total on-source time is  $\sim 44$  hours. The phase tracking center of our observation is  $\alpha(\text{J2000}) = 6^{\text{h}}18^{\text{m}}37^{\text{s}}.6$ ,  $\delta(\text{J2000}) = 78^{\circ}21'24''.1$ . We used tunerless SIS receivers (Sunada et al. 1994), and observed the  $^{12}\text{CO}(1-0)$  line in the upper side band. Double side band system temperature was about 200 – 300 K for most of the observations. The backend used was the XF-type spectro-correlator Ultra Wide Band Correlator (UWBC; Okumura et al. 2000), configured to have 512 MHz bandwidth with 256 channels (i.e., a 2 MHz channel width or  $5.2 \text{ km s}^{-1}$  velocity resolution). We observed 3C279 as a bandpass calibrator, and 0633+734 as an amplitude and phase calibrator. The flux scale of 0633+734 was determined by comparisons with Mars, Uranus, and Neptune, and the uncertainty in the absolute flux scale is estimated to be  $\sim 10\%$ .

The data were calibrated using the NRO software package “UVPROC II” (Tsutsumi et al. 1997), and were CLEANed using standard procedures implemented in the NRAO software *AIPS*. The maps were made with natural weighting, with a final synthesized beam size of  $3''.4 \times 2''.8$  ( $280 \text{ pc} \times 230 \text{ pc}$ ) and a position angle of  $108^{\circ}$ . The noise level of the full spectral resolution maps ( $5.2 \text{ km s}^{-1}$ ) is  $11.4 \text{ mJy beam}^{-1}$ . The noise level of the  $20.8 \text{ km s}^{-1}$  resolution channel maps in figure 2 is  $5.7 \text{ mJy beam}^{-1}$ .

### 3. Results

#### 3.1. Overall Molecular Gas Distribution and Kinematics

In figure 1, we present the  $^{12}\text{CO}(1-0)$  integrated intensity (moment 0, figure 1a) and the intensity-weighted mean velocity field (moment 1, figure 1b) maps of the central region of NGC 2146. Most of the CO emission is concentrated along the galactic disk with the inner CO intensity peaks of the image roughly following the major axis, but with the outer regions of the galactic disk clearly tilted counter-clockwise from the major axis. These features are consistent with previous interferometric  $^{12}\text{CO}(1-0)$  observations (Jackson & Ho 1988; Greve et al. 2000; Greve et al. 2006). The velocity field (figure 1b) shows that the overall velocity contours are roughly symmetric, although here, as well, a tilt is present at the outer part of the galactic disk. The position angle of this galaxy, derived from its kinematics (i.e., from the velocity field), is  $137^\circ$  (an angle of  $0^\circ$  corresponds to north, increasing counterclockwise). This value is consistent with that derived from past CO observations ( $135^\circ$ ; Dumke et al. 2001). Figure 2 shows the  $^{12}\text{CO}(1-0)$  channel maps of the same region with a velocity resolution of  $20.8 \text{ km s}^{-1}$ . The overall molecular gas features along the galactic disk (P.A. of  $137^\circ$ ) are similar to those often seen in galaxies with flat-rotation curves. In addition, there are some diffuse structures outside the galactic disk.

The position-velocity ( $p-v$ ) diagram taken along the major axis (figure 3) can be fitted in the central region of the galactic disk by two rigid body rotation curves. The rigid body rotation curve between  $-4''$  and  $+4''$  shows a steeper gradient than that between  $-10''$  and  $+10''$ . Since the former structure is located closer to the nucleus of the galaxy, hereafter we refer to it as the “nuclear disk”, while the latter is referred to as the “inner disk”. The region outside the inner disk (hereafter called the “outer disk”) shows flat rotation.

The total CO flux density detected in figure 1a is measured as  $\sim 1.8 \times 10^3 \text{ Jy km s}^{-1}$  ( $= 110 \text{ K km s}^{-1}$ ). The CO luminosity over a  $1 \times 10^7 \text{ pc}^2$  area is then calculated as  $1.1 \times 10^9 \text{ K km s}^{-1} \text{ pc}^2$ . The CO luminosities observed with the IRAM 30 m single dish telescope and the Plateau de Bure Interferometer are  $(1.2 \pm 0.1) \times 10^9 \text{ K km s}^{-1} \text{ pc}^2$  over  $1 \times 10^7 \text{ pc}^2$  area and  $0.8 \times 10^9 \text{ K km s}^{-1} \text{ pc}^2$  over  $0.8 \times 10^7 \text{ pc}^2$  area, respectively (with their values re-scaled because of the different distance for NGC 2146 adopted by us; Greve et al. 2006). If we allow for a calibration error of 10% in our data, our CO luminosity is comparable with the single dish luminosity reported in Greve et al. (2006), indicating that our observations recovered all the CO flux, and hence, are not affected by the missing flux problem.

#### 3.2. Large-Scale Expanding Molecular Superbubble and Outflow

In addition to the bright features seen in the galactic disk region, we also detected diffuse and extended structures above and below the galactic disk. These features are labelled *OF1* and *SB1* in figure 1a. In figure 1b, these regions show velocity structures more disturbed than

the disk region, and obvious deviation from symmetric velocity contours can be easily seen.

Figure 4 is a  $p - v$  diagram along the minor axis after the molecular gas data have been integrated along the major axis (see figure 5 for the range over which the integration has been performed). The  $p - v$  diagram shows that most of the molecular gas is concentrated in the central “vertical” region at the position of zero arcsec, which corresponds to the galactic disk. Outside of the disk, however, the two diffuse and extended structures, *SB1* and *OF1* are also evident. The arc *SB1* shows a half shell-like structure encompassing a cavity, which corresponds to the *SB1* in figure 1a. A similar half shell-like molecular structure seen in the  $p - v$  diagrams of M82 has been explained in terms of an expanding bubble (Neininger et al. 1998; Weiss et al. 1999; Wills et al. 1999). Comparable behavior has often been reported in expanding HI superbubbles (Deul & den Hartog 1990). The similarities between the distribution and kinematics of *SB1* and those of the expanding bubbles reported in literature lead us to conclude that *SB1* is indeed an expanding molecular superbubble. From the integrated intensity map (figure 1a) and the major-axis-integrated  $p - v$  diagram (figure 4), we can estimate the radius of *SB1* to be  $\sim 10'' - 15''$ , which corresponds to  $\sim 800 - 1200$  pc at a distance of 17.2 Mpc. The range of the radius depends on where we assume the center of the bubble is located; the minimum radius corresponds to the edge of the disk, and the maximum the center of the disk. The expansion velocity can also be measured from the  $p - v$  diagram. We assume that the superbubble expansion is traced by the intensity peaks marked by the red dashed line of figure 4. In this case, the measured expansion velocity is  $\sim 50 \pm 10$  km s $^{-1}$ .

Following the arrow overlapped to the extended region *OF1* (seen as an arc in figure 1a), a velocity gradient is seen. Similar features with linear increasing velocity are often seen in outflows from young stellar objects in star forming regions in our Galaxy. Because of the location, structure, and kinematics of the arc *OF1*, we conclude that *OF1* is most likely an outflow. This linear feature in figure 4 extends from the center of the galaxy to a position  $\sim 25''$  distant from it, hinting at an extension of the outflow from the galactic center of  $\sim 2$  kpc. Near the galactic disk, both blueshifted and redshifted components can be seen (within  $\pm 150$  km s $^{-1}$ , between two red solid lines in the right side of figure 4). The outflow velocity is increasing linearly from  $V_{LSR}$  of  $\sim 0$  km s $^{-1}$  to  $\sim +200$  km s $^{-1}$ .

From *SB1* in figure 1b, a diffuse linear structure with a very small velocity gradient is pointing toward the south. This structure can also be clearly seen in the channel maps (figure 2) at a velocity range between 829.8 km s $^{-1}$  and 850.6 km s $^{-1}$ . This component matches with the CO clumps reported in Karlsson et al. (2004), and is probably associated with a dust lane or “dust finger” stretching southwest from the galactic center (Young et al. 1988; Hutchings et al. 1990; Greve et al. 2000).

### 3.3. Smaller-Scale Molecular Superbubbles

Together with the two aforementioned diffuse structures, which are obvious in the integrated intensity map and the  $p-v$  diagram, there is another bubble-like structure detected around the galactic disk region. The molecular gas in normal circular galactic rotation would be concentrated along a rigid- or flat-rotation curve. Gas not exhibiting this behavior can be considered as gas rotating under non-circular motion or moving under different mechanisms.

Figure 6 shows the  $p-v$  diagrams along the major axis with different offsets. Most of the molecular gas is indeed concentrated along the rigid- or flat-rotation curves, but some diffuse structures can be seen away from these curves. All of the diffuse structures appear only to the west of the galactic center with its offset between  $-5.''0$  and  $-16.''0$  from the nucleus (the vertical dashed lines in figure 6). Since non-circular motion, such as gas along a bar, generally has a symmetric structure, we think that these structures in NGC 2146 may be produced by another mechanism. Therefore, we averaged the  $p-v$  diagram between  $-4.8''$  and  $0''$  offset from the major axis (figure 7). The outcome clearly shows a diffuse shell-like structure, indicated by the red dashed curve labelled *SB2* in figure 7, only at the western side of the galactic center. Hence, this feature in the  $p-v$  diagram can be explained with an expanding molecular superbubble such as that in *SB1* mentioned above.

A close look at this superbubble shows two inner cavities, indicated by red plus symbols in figure 7. The velocities associated with  $p1$  and  $p2$  are  $+20 \text{ km s}^{-1}$  and  $-5 \text{ km s}^{-1}$  relative to the systemic velocity, respectively. The diffuse structures around  $p1$  can be also seen in the  $p-v$  diagrams (figure 6) from the positions  $-5.''0$  to  $+3.''0$  offset from the major axis, and those around  $p2$  appear from  $-5.''0$  to  $0.''0$  relative to the major axis. Furthermore, most of the  $p-v$  diagrams in figure 6 show that the molecular gas avoids the positions  $p1$  and  $p2$ , resulting in shell-like structures. From these figures, we can infer two independent superbubbles at  $p1$  and  $p2$ . However, the signal-to-noise ratio difference between these two cavities is small, only about  $2\sigma$  difference, and therefore it is more natural to consider these structures to be created by the same explosion event. In this case, the structure dividing  $p1$  and  $p2$  is just a detail feature of one molecular bubble or possibly just noise in our data. In addition, the positions of  $p1$  and  $p2$  lie away from the rigid- or flat-rotation part where most of the molecular gas resides, and hence, we consider the possibility that the molecular bubbles originate from these points to be less likely. Therefore, in the following, we will consider *SB2* as one superbubble, which is  $\sim 10''$  offset from the galactic center (figure 7).

From figures 5, 6, and 7, we can estimate the main characteristics of *SB2*: Its radius is estimated to be  $\sim 5'' - 13''$  ( $400 - 1000 \text{ pc}$ ), and the expansion velocity is measured as  $\sim 35 \pm 10 \text{ km s}^{-1}$ . The range of the radius depends again on where we assume the center of the bubble to lie; the minimum radius corresponds to the edge of the disk, and the maximum to the plane of the disk, respectively.



#### 4. Search for Bubbles or Outflows by Velocity Model Subtraction

In the previous section, we have reported convincing arguments in favor of the presence in NGC 2146 of two molecular bubbles and an outflow derived using the integrated intensity maps and the  $p - v$  diagrams. In the following, we will focus on a search for bubbles and/or outflows within the galactic disk of NGC 2146 using a ‘model subtraction’ method.

The model we have used can be described as follows: We first use the *AIPS* task *IRING* to compute mean intensity within a range of azimuthal angles per a certain radius range of a ring to obtain the velocity information. We calculate the mean intensity within  $10^\circ$  of the major axis for each redshifted and blueshifted velocity range (see figure 5). We then fit the  $p - v$  diagram along the major axis with an Elmegreen curve (Elmegreen & Elmegreen 1990), parametrized as:

$$v = \frac{r}{(r^\alpha + r^{1-\beta})} \times \gamma, \quad (1)$$

where  $v$  is the rotational velocity in units of  $\text{km s}^{-1}$ ,  $r$  is the galactocentric radius in units of kpc, and the variables  $\alpha$ ,  $\beta$ , and  $\gamma$  are the free parameters. Figure 8 shows the data and the fit, and the results of the fit are  $\alpha = 0.30$ ,  $\beta = 0.32$ , and  $\gamma = 256.39$ .

To characterize the galactic kinematics of the central region of NGC 2146, we compare the observed kinematics with the large-scale galactic rotation. Figure 9a presents the  $p - v$  diagram along the major axis overplotted with the fitted rotation curve (from figure 8). We have further modeled the velocity map from the fitted rotation curve under the assumption that the galactic disk is axisymmetric with an inclination angle of  $63^\circ$  (Della Ceca et al. 1999). Figure 9b shows this modeled velocity map overlaid with the observed velocity map. An excellent agreement between these two maps is seen. We then subtract the modeled velocity map from our NMA velocity map, and show the resultant residual velocity map in figure 9c and the residual velocity along the major axis in figure 9d. The residual velocities along the major axis are, on average, less than  $\pm 5 \text{ km s}^{-1}$  (comparable to our velocity resolution) with maximum residual velocities of only  $\pm 10 \text{ km s}^{-1}$ . In addition, the residual velocities over the entire galactic disk region are never larger than about  $\pm 20 \text{ km s}^{-1}$ . There are some systematic residual velocities around  $\pm 4''$  from the center with a negative residual velocity around the position of  $+4''$ , and positive residual velocity around the position of  $-4''$ . Since these regions correspond to those where there are two rigid-rotation components (see figure 3), a simple Elmegreen rotation curve does not constitute an optimal fit. These systematic residual velocities are therefore an artificial effect, and should not be considered as an outflow feature. From these results, we have concluded that the galactic kinematics within a few kpc of the central region of NGC 2146 can be described by normal galactic rotation. We find no evidence of outflows with velocities greater than  $20 \text{ km s}^{-1}$  in the galactic disk. Note that our model subtraction method does not detect any evidence of *SB2*. This is because our method uses an

intensity-weighted mean velocity field map, and therefore diffuse and weak components, such as *SB2*, cannot be detected.

HI absorption line observations have revealed that the central region of NGC 2146 is undisturbed and smooth, and can be interpreted as a rotating disk (Tarchi et al. 2004), which is consistent with our results. The overall CO distributions in our channel maps are similar to those shown in Greve et al. (2000). Some of the structures in the channel maps have been interpreted by Greve et al. (2000) as outflow features (thick solid lines in their figures 6 and 8c). Our velocity model fitting indicates that those structures may be explained instead by normal galactic rotation.

## 5. Properties of the Molecular Superbubbles and the Outflow

In this section, we calculate the timescales, masses, and energies of the molecular superbubbles and the outflow present in NGC 2146. The molecular and total gas masses, in unit of  $M_{\odot}$ , can be calculated as

$$M_{\text{H}_2} = 1.2 \times 10^4 \times D^2 \times S_{\text{CO}(1-0)} \times \frac{X_{\text{CO}}}{3.0 \times 10^{20}}, \quad (2)$$

$$M_{\text{gas}} = 1.36 \times M_{\text{H}_2}, \quad (3)$$

where  $D$  is the distance in units of Mpc,  $S_{\text{CO}(1-0)}$  is the CO integrated intensity in units of Jy km s<sup>-1</sup>,  $X_{\text{CO}}$  is the CO-to-H<sub>2</sub> conversion factor in units of cm<sup>-2</sup> (K km s<sup>-1</sup>)<sup>-1</sup>, and the factor 1.36 is to account for the presence of elements other than hydrogen (Sakamoto et al. 1995). In the following calculations, we assumed the  $X_{\text{CO}}$  to be  $1.4 \times 10^{20}$  cm<sup>-2</sup> (K km s<sup>-1</sup>)<sup>-1</sup>, which is the same value as that used for the molecular gas mass calculations in M82 (Matsushita et al. 2000) with which NGC 2146 shares a number of similarities (see section 1). We also assume that the energy of one supernova explosion is  $\sim 1 \times 10^{51}$  erg (Rose 1998). All the derived values are summarized in table 1. Note that the total gas mass derived from our observation (with  $S_{\text{CO}(1-0)} \sim 1.8 \times 10^3$  Jy km s<sup>-1</sup>; see section 3.1) is  $\sim 4.1 \times 10^9 M_{\odot}$ .

### 5.1. Properties of Molecular Superbubbles

First, we discuss the molecular superbubble *SB1*, which is shown in figure 1 and 4. If we assume that the expansion velocity stayed constant since the beginning of the superbubble's expansion, we can derive its dynamical timescale,  $t_{\text{SB1}}$ . Using the radius of  $\sim 800 - 1200$  pc and the expansion velocity of  $50 \pm 10$  km s<sup>-1</sup>, we obtain the timescale  $t_{\text{SB1}} = (800 - 1200 \text{ pc}) / (50 \pm 10 \text{ km s}^{-1}) \sim (1.3 - 2.9) \times 10^7$  years. The integrated intensity of *SB1* is 115 Jy km s<sup>-1</sup>, so from equations (2) and (3), the gas mass of *SB1* is calculated to be  $\sim 2.6 \times 10^8 M_{\odot}$ . The kinetic energy of the superbubble,  $E_{\text{SB1}}$ , is therefore estimated to be  $E_{\text{SB1}} = \frac{1}{2} \times (2.6 \times 10^8 M_{\odot}) \times (50 \pm 10 \text{ km s}^{-1})^2 \sim (4.1 - 9.3) \times 10^{54}$  erg. Considering that  $\sim 10 - 20$  % of the energy transmits from supernova explosions into the surrounding ISM (McCray & Kafatos 1987; Weaver et al. 1977; Larson 1974), 20,500 – 93,000 supernova explosions are required to account for the energy



of *SB1*.

Second, we estimate the properties of the molecular superbubble *SB2*, which is shown in figures 5, 6, and 7. Again, with the same assumption of constant expansion velocity and using the radius of  $\sim 400 - 1000$  pc (see section 3.3), we can derive the timescale,  $t_{\text{SB2}} = (400 - 1000 \text{ pc}) / (35 \pm 10 \text{ km s}^{-1}) \sim (0.9 - 3.9) \times 10^7$  years. The integrated intensity of *SB2* measured from the  $p - v$  diagram is  $17.3 \text{ Jy km s}^{-1}$ , so that the mass of *SB2* is calculated as  $\sim 3.9 \times 10^7 M_{\odot}$ . In this case, the energy of the bubble,  $E_{\text{SB2}}$ , is estimated as  $E_{\text{SB2}} = \frac{1}{2} \times (3.9 \times 10^7 M_{\odot}) \times (35 \pm 10 \text{ km s}^{-1})^2 \sim (2.4 - 7.9) \times 10^{53}$  erg. After applying the efficiency of 10 – 20%, the energy corresponds to 1,200 – 7,900 supernova explosions.

The size, expansion timescales and velocities are similar for both superbubbles, but the mass and therefore the energy derived for *SB1* are about an order of magnitude larger than for *SB2*. These results may suggest that *SB1* is related to a more active (energetic) starburst than that related to *SB2*.

### 5.2. Properties of the Molecular Outflow “*OF1*”

Since the  $p - v$  diagram shows a linear increase in velocity as a function of the distance from the galactic disk for this molecular outflow *OF1* (see section 3.2), it is natural to assume that *OF1* is experiencing a constant acceleration. Using a size and a terminal velocity for the outflow of 2 kpc and  $200 \text{ km s}^{-1}$ , respectively, the acceleration,  $a_{\text{OF1}}$ , and the timescale,  $t_{\text{OF1}}$ , of the outflow can be calculated as  $a_{\text{OF1}} = \frac{1}{2} \times (200 \text{ km s}^{-1})^2 / (2 \text{ kpc}) \sim 3.2 \times 10^{-13} \text{ km s}^{-2}$  and  $t_{\text{OF1}} = (200 \text{ km s}^{-1}) / (3.2 \times 10^{-13} \text{ km s}^{-2}) \sim 2.0 \times 10^7$  years, respectively. On the other hand, it is also possible to assume that the initial expansion velocity of the outflowing gas is different in each gas cloud. Therefore faster (slower) gas is located far from (close to) the galactic disk, resulting in the linear increase in velocity as a function of the distance from the galactic disk in the  $p - v$  diagram. In this case, the timescale of *OF1* can be estimated from the furthest distance of *OF1* and its velocity as,  $t'_{\text{OF1}} = (2 \text{ kpc}) / (200 \text{ km s}^{-1}) \sim 1.0 \times 10^7$  years. Both assumptions lead to the similar timescales. The integrated intensity of *OF1* is estimated to be  $150 \text{ Jy km s}^{-1}$ , leading to a total mass for the outflow of  $3.4 \times 10^8 M_{\odot}$  (see equations 2 and 3).

According to the kinematics described above, the molecular outflow velocity is not constant like in the case of the two molecular bubbles *SB1* and *SB2*. Hence, the outflow energy,  $E_{\text{OF1}}$  has to be calculated from each channel map according to the relation  $E_{\text{OF1}} = \sum_i \frac{1}{2} m_i v_i^2$ , where  $m_i$  and  $v_i$  are the molecular gas mass and the velocity of *OF1* at each channel  $i$ . The energy is calculated as  $E_{\text{OF1}} \sim 3.0 \times 10^{55}$  erg. After applying the efficiency of 10 – 20%, it corresponds to 150,000 – 300,000 supernova explosions.

## 6. Discussion

### 6.1. Soft X-ray Emission from the Large-Scale Molecular Bubble and Outflow

NGC 2146 has a kpc-scale outflow from the galactic center detected at soft X-ray wavelengths (Inui et al. 2005; Armus et al. 1995). Here, we compare our  $^{12}\text{CO}(1-0)$  map with the soft X-ray image obtained with the Chandra X-ray Observatory (Inui et al. 2005). Figure 10 shows the  $^{12}\text{CO}(1-0)$  integrated-intensity contour map overlaid on the soft X-ray image. The soft X-ray image shows strong extended emission toward the northeastern part of the galaxy, and weak extended emission in the southwest. Between these two diffuse emission regions, there is almost no emission except for a number of strong point sources. The latter location corresponds to the strong CO emitting region, namely the galactic disk region, and therefore the lack of diffuse soft X-ray emission can be explained by absorption from the molecular gas in the galactic disk. Because the stronger X-ray emission appears in the northeastern region of the galactic disk rather than in the southwestern region, the most probable picture is that the southwestern edge of the CO emission is at the near side of the galactic disk and the northeastern one is at the far side. This scenario is indeed consistent with previous studies (Armus et al. 1995; Greve et al. 2000).

Since the soft X-ray image traces the location of hot thermal plasma in this galaxy (Armus et al. 1995; Della Ceca et al. 1999; Inui et al. 2005), the comparison between our  $^{12}\text{CO}(1-0)$  map and the soft X-ray map gives the schematic image of the relative location between the molecular gas and the hot plasma. In figure 10, the northeastern X-ray emission shows a conical structure, emanating from the center of the galaxy and spreading outwards, perpendicular to the major axis of the galaxy (color-scale features enclosed by two red shorter dashed lines). The molecular outflow, *OF1*, is located around the front edge of the X-ray outflow. This fact and the good spatial correspondence suggest that these two outflows are physically connected.

We then compared the molecular gas outflow energy with that of the soft X-ray outflow. As reported in section 5.2 (and in Table 1), the energy of *OF1* is calculated as  $E_{\text{OF1}} \sim 3.0 \times 10^{55}$  erg. On the other hand, the energy of the thermal plasma outflow is estimated as  $E_{\text{X}} = 5.1 \times 10^{56} f^{\frac{1}{2}}$  erg (with their value re-scaled because of the different distance for NGC 2146 adopted by us; Inui et al. 2005), where  $f$  is the volume filling factor for the X-ray emitting gas. If we adopt the standard value of 0.01 – 0.1 for  $f$  (Armus et al. 1995), the thermal plasma outflow energy can be calculated as  $(0.5 - 1.6) \times 10^{56}$  erg. The energy of the thermal plasma outflow is therefore comparable or an order of magnitude larger than the molecular outflow energy, depending on the volume filling factor for the X-ray emitting gas. The thermal plasma would therefore have enough energy to push *OF1* out from the galactic disk.

We also compared the pressure of the molecular gas in the outflow with that of the soft X-ray outflow. The molecular gas pressure can be measured by  $P_{\text{mol}} \sim n(\text{H}_2)k_{\text{B}}T$ , where

$n(\text{H}_2)$  is the  $\text{H}_2$  gas number density,  $k_{\text{B}}$  is the Boltzmann constant, and  $T$  is the molecular gas temperature. Since our observations do not provide any density or temperature information, here we assume standard values, namely a molecular gas density and temperature traced by  $^{12}\text{CO}(1-0)$  of  $10^{2-3} \text{ cm}^{-3}$  and  $10 - 100 \text{ K}$ , respectively. Thus the molecular gas pressure is estimated as  $\sim 1.4 \times 10^{(-12\pm 1)} \text{ dyne cm}^{-2}$ . The thermal plasma outflow pressure is estimated as  $P_{\text{X}} = (1.0 - 3.2) \times 10^{-11} \text{ dyne cm}^{-2}$  with the volume filling factor of  $0.1 - 0.01$  (Inui et al. 2005), the pressure of the thermal plasma outflow is therefore comparable or two orders of magnitude larger than that of the molecular outflow, depending on the volume filling factor for the X-ray emitting gas and the density and/or temperature of the molecular gas. This result further supports the capability of the thermal plasma to push *OF1* out from the galactic disk. Since the energy and the pressure of the X-ray emission is larger than that of the molecular outflow, it is natural to consider that the expanding force from X-ray emission is still pushing the surrounding molecular gas.

The distribution, kinematics, energies, and pressure of the molecular gas and the hot thermal plasma outflows suggest that the hot thermal plasma pushes the molecular gas outward, and produces the large-scale outflows. The hot thermal plasma is caused by supernova explosions in the central starburst region of NGC 2146 (e.g., Armus et al. 1995) and, very likely, the molecular gas outflow is also caused by the intense starbursts at the center of NGC 2146 (Greve et al. 2000). Furthermore, the arc-like feature of *OF1*, with the conical structure of the hot thermal plasma outflow just behind *OF1*, suggests that the molecular outflow could have had a bubble-like structure at the beginning of the expansion, and then been blown out as an arc-like feature as it evolved. Indeed, the molecular superbubble with hot gas inside observed in the central region of M82 (Matsushita et al. 2005) could well represent an analogue of *OF1* at an early stage.

Two-dimensional hydrodynamical simulations (e.g., Tomisaka & Ikeuchi 1988) support the evolution of a molecular superbubble to an outflow. One of their models simulated the evolution of a superbubble under the ISM density of  $100 \text{ cm}^{-3}$ , which corresponds to that of molecular gas seen in  $^{12}\text{CO}(1-0)$ . Supernova explosions at a constant rate for a long time produce a vast amount of hot gas, and the hot gas accelerates and expands the surrounding ISM gradually. This model shows that the size of the molecular superbubble can expand to  $\sim 2 \text{ kpc}$  on a timescale of  $\sim 10^7$  years. Since the supernova rate (SNR) of this model adopts that of M82 ( $0.1 \text{ yr}^{-1}$ ), and NGC 2146 has a similar SNR ( $0.15 \text{ yr}^{-1}$ ; Tarchi et al. 2000), this model can be considered valid for NGC 2146. Furthermore, the values of the size and the timescale from this model are similar to our observations, and therefore our results are consistent with the model.

At the center of the expanding molecular bubble *SB1*, diffuse soft X-ray emission, indicative of hot thermal plasma, seems to be present. Figure 10 show two soft X-ray images with different spatial resolutions: Figure 10a is the higher spatial resolution image, where point

sources are clearly visible, while it is more difficult to see the diffuse components. Figure 10b is the lower spatial resolution image, where diffuse components are more clearly seen. Comparison of these two images can separate point sources and diffuse sources, and indeed at the center of *SB1*, diffuse soft X-ray emission is detected. This situation is again similar to that observed in M82 and expected from hydrodynamical simulations, suggesting that the hot gas is embedded inside of the expanding molecular bubble *SB1*, pushing the surrounding molecular gas outward. A precise estimate of the energy of the soft X-ray component is, however, difficult since, in this region, the soft X-ray emission is absorbed by the foreground molecular gas and, therefore, any value derived for the energy would be significantly underestimated.

## 6.2. Configurations of Outflows and Bubbles

Here we discuss the possible configuration of the outflows and bubbles in the central  $60''$  of NGC 2146 based on our CO and X-ray data, and the previously published optical spectra. A schematic diagram of the possible configuration of the molecular gas and other components is shown in figure 11 and, in the following paragraphs, its details are discussed.

As shown in section 4, the molecular gas disk is well modeled by the standard rigid- and flat-rotation curves with an inclination of  $63^\circ$ . Based on this simple regular galactic kinematics, it is safe to assume that the galactic disk is flat and has no warp in the central region. Comparison between the CO in the galactic disk and the X-ray data indicates that the outflow is directed toward us in the northeastern side, and the CO in the galactic disk in “blocking” the soft X-ray emission in the southwestern side, making that the near side (Sect. 6.1). Indeed, the long-slit optical spectra along the minor axis show that the ionized gas is blueshifted to the northeast and redshifted to the southwest, and the spectra taken in the central  $2''$  show a blue asymmetry in the emission lines, suggesting that the ionized gas outflow is flowing toward us in the northeast, and the redshifted outflow is blocked by the galactic disk around the galactic center (Armus et al. 1995), which is consistent with the configuration we propose.

The soft X-ray outflow shows a conical structure with a large opening angle (see figure 10), and the outflowing direction is inclined toward us. From the blue asymmetry in the optical spectra near the galactic center, the line-of-sight ionized gas outflow velocity toward us is estimated as  $\sim 300 - 400 \text{ km s}^{-1}$  (Armus et al. 1995). The redshifted side, on the other hand, shows only  $\sim 100 \text{ km s}^{-1}$  (estimated from figure 11 of Armus et al. 1995), suggesting that the far side of the conical structure of the outflow is nearly perpendicular to the line-of-sight. *OF1* is dominated by the redshifted gas, suggesting that most of the molecular gas is located at the far side of the conical structure. The line width of ionized gas increases with distance to the galactic center (Armus et al. 1995), suggesting an acceleration as the gas moves away, consistent with the kinematics of *OF1*.

*SB1* is located in the southwestern part of the galaxy, indicating that *SB1* is at the farside of the galactic disk. The radius of the molecular gas disk is about 2 kpc (about  $25''$ )

with an inclination of  $63^\circ$ , while the central velocity of *SB1* is somewhat blueshifted and the radius of *SB1* is about  $\sim 1$  kpc. Therefore, in order to be able to partially see *SB1*, this has to be closer to us than the galactic center.

Summing up all the aforementioned information, we made a schematic diagram of the possible configuration of the molecular gas and the hot gas outflows in figure 11. In the figure, the molecular gas is shown in red, X-ray emission in yellow, and optical emission line in light blue. The emission obscured by the molecular gas (and possibly dust that is mixed with the molecular gas) in front is shaded. The overall configuration of this schematic diagram is globally consistent with that presented in Greve et al. (2000) but, by using our new observations, we have been able to describe the different structures and components presented in the inner region of NGC 2146 in greater detail.

In sections 5.1 and 5.2, we derive the properties of *SB1* and *OF1*. Since the timescale of *SB1* corresponds roughly to that of *OF1*, it is possible that *SB1* and *OF1* originated from one starburst event. The difference in the structure (*SB1* is still a bubble while *OF1* is already outflowing) can be explained by the possible location where the starburst may have started up; if a starburst occurred a bit above the galactic disk plane, an expansion upward is less frustrated than downward due to a less dense ISM. Since a bubble expands faster in less dense conditions (Tomisaka & Ikeuchi 1988), an expansion in a lower density ISM leads to faster bubble evolution, and the bubble becomes an outflow earlier than that in a dense region. However, the possible central locations for *SB1* and *OF1* are different (figure 1; see also figure 11), it is difficult to say that *SB1* and *OF1* have the same explosion center. Thus it is safer to conclude that *SB1* and *OF1* may have formed in the same explosion period, but at different locations.

## 7. Summary

We observed the nearby nearly edge-on starburst galaxy NGC 2146 with the NMA in the  $^{12}\text{CO}(1-0)$  line. We performed a deep integration and successfully imaged a diffuse molecular outflow (*OF1*) and two superbubbles (*SB1* and *SB2*), expanding from the galactic disk region.

*OF1* is located toward the northeastern side of the galactic disk and shows a linear increase in velocity with the distance from the galactic disk. It shows an arc-like feature, and is located at the front edge of the soft X-ray outflow. The energy of *OF1* is comparable to or an order of magnitude lower than that of the soft X-ray outflow. The pressure of *OF1* is about one or two orders of magnitude lower than that of the soft X-ray outflow. Therefore these results suggest that *OF1* is pushed outward by the energetic plasma outflow from the galactic disk.

*SB1* is located at the southwestern side of the galactic disk and shows an expanding motion. The soft X-ray image shows diffuse and weak emission at the center of *SB1*. Since *SB1* is located on the far side of the galactic disk from us, this weakness is likely due to the soft X-ray emission being highly absorbed by the galactic disk. It is not clear whether the soft X-ray emission can be the energy source of the expansion of *SB1*. The lifetime of *SB1* and

*OF1* are similar, and hence, we think that these structures have been formed during the same explosion period. *SB2* is clearly visible in the position-velocity diagram, and has less mass than *SB1*, and is therefore less energetic than *SB1*. Possibly *SB2* has been caused by a less energetic starburst than the one that produced *OF1* or *SB1*.

The galactic disk seems to have two rigid-rotating components and one flat-rotating component. The inner rigid-rotating component has a steeper velocity gradient than the outer rigid-rotating component, and is  $\sim 300$  pc in radius, indicating that there is a fast rotating nuclear disk in this galaxy. Model fitting to the velocity field maps shows that the central region of the galactic disk of NGC 2146 can be explained by regular galactic rotation, and there is no clear evidence for molecular gas tracing an outflow inside the galactic disk.

We appreciate to Paul T. P. Ho, You-Hua Chu, and the anonymous referee for very useful comments. We also grateful to the NRO staff for the operation and improvement of the NMA. This work is supported by the National Science Council (NSC) of Taiwan, NSC 96-2112-M-001-009 and NSC 97-2112-M-001-021.

## References

- Armus, L., Heckman, T. M., Weaver, K. A., & Lehnert, M. D. 1995, *ApJ*, 445, 666  
Benvenuti, P., Capaccioli, M., & D’Odorico, S. 1975, *A&A*, 41, 91  
Dahlem, M., Weaver, K. A., & Heckman, T. M. 1998, *ApJS*, 118, 401  
Della Ceca, R., Griffiths, R. E., Heckman, T. M., Lehnert, M. D., & Weaver, K. A. 1999, *ApJ*, 514, 772  
Deul, E. R., & den Hartog, R. H. 1990, *A&A*, 229, 362  
Dumke, M., Nieten, Ch., Thuma, G., Wielebinski, R., & Walsh, W. 2001, *A&A*, 373, 853  
Elmegreen B. G. & Elmegreen D. M. 1990, *ApJ*, 355, 52  
Fisher, J. R., & Tully, R. B. 1976, *A&A*, 53, 397  
Greve, A., Neininger, N., Sievers, A., & Tarchi, A. 2006, *A&A*, 459, 441  
Greve, A., Neininger, N., Tarchi, A., & Sievers, A. 2000, *A&A*, 364, 409  
Handa, T., Sofue, Y., Ikeuchi, S., Kawabe, R., & Ishizuki, S. 1992, *PASJ*, 44, L227  
Hutchings, J. B., Neff, S. G., Stanford, S. A., Lo, E., & Unger S. W. 1990, *AJ*, 100, 60  
Inui, T., Matsumoto, H., Tsuru, T. G., Koyama, K., Matsushita, S., Peck, A. B., & Tarchi, A. 2005, *PASJ*, 57,135  
Irwin, J. A. & Sofue, Y. 1996, *ApJ*, 464, 738  
Jackson, J. M., & Ho, P. T. P. 1988, *ApJL*, 324, L5  
Karlsson, E., Aalto, S., & Bergman, P. 2004, *ASP Conf. Ser.*, 320, 158  
Larson, R. B. 1974, *MNRAS*, 169, 229  
Lehnert, M. D., & Heckman, T. M. 1996, *ApJ*, 462, 651  
Marcolini, A., Strickland, D. K., D’Ercole, A., Heckman, T. M., & Hoopes, C. G. 2005, *MNRAS*, 362, 626



- Martin, C. L. 1998, *ApJ*, 506, 222
- Matsushita, S., Kawabe, R., Kohno, K., Matsumoto, H., Tsuru, T. G., & Vila-Vilaró, B. 2005, *ApJ*, 618, 712
- Matsushita, S., Kawabe, R., Matsumoto, H., Tsuru, T. G., Kohno, K., Morita, K.-I., Okumura, S. K., & Vila-Vilaró, B. 2000, *ApJ*, 545, L107
- McCray, R. & Kafatos, M. 1987, *ApJ*, 317, 190
- Nakai, N., Hayashi, M., Handa, T., Sofue, Y., Hasegawa, T., & Sasaki, M. 1987, *PASJ*, 39, 685
- Neininger, N., Guélin, M., Klein, U., García-Burillo, S., & Wielebinski, R. 1998, *A&A*, 339, 737
- Okumura, S. K., et al. 2000, *PASJ*, 52, 393
- Rand, R. J. 2000, *ApJ*, 535, 663
- Rose, W. K. 1998, *Advanced Stellar Astrophysics* (Cambridge: Cambridge University Press)
- Sakamoto, K., et al. 2006, *ApJ*, 636, 685
- Sakamoto, K., Okumura, S., Minezaki, T., Kobayashi, Y., & Wada, K. 1995, *AJ*, 110, 2075
- Sanders, D. B., Mazzarella, J. M., Kim, D.-C., Surace, J. A., & Soifer, B. T. 2003, *AJ*, 126, 1607
- Strickland, D. K., Heckman, T. M., Colbert, E. J. M., Hoopes, C. G., & Weaver, K. A. 2004, *ApJ*, 606, 829
- Strickland, D. K., & Stevens, I. R. 2000, *MNRAS*, 314, 511
- Sunada, K., Kawabe, R., & Inatani, J. 1994, *Int. J. Infrared Millimeter Waves*, 14, 1251
- Taramopoulos, A., Payne, H., & Briggs, F. H. 2001, *A&A*, 365, 360
- Tarchi, A., Greve, A., Peck, A. B., Neininger, N., Wills, K. A., Pedlar, A., & Klein, U. 2004, *MNRAS*, 351, 339
- Tarchi, A., Neininger, N., Greve, A., Klein, U., Garrington, S. T., Muxlow, T. W. B., Pedlar, A., & Glendenning, B. E. 2000, *A&A*, 358, 95
- Tenorio-Tagle, G., & Bodenheimer, P. 1988, *ARA&A*, 26, 145
- Tomisaka, K., & Ikeuchi, S. 1988, *ApJ*, 330, 695
- Tsutsumi, T., Morita, K.-I., & Umeyama, S. 1997, in *ASP Conf. Ser. 125, Astronomical Data Analysis Software and Systems VI*, ed. G. Hunt & H. E. Payne (San Francisco: ASP), 50
- Tully, R. B. 1988, *Nearby Galaxies Catalog* (Cambridge: Cambridge University Press)
- Walter, F., Dahlem, M., & Lisenfeld, U. 2004, *ApJ*, 606, 258
- Weaver, R., McCray, R., & Castor, J. 1977, *ApJ*, 218, 377
- Weiss, A., Neininger, N., Hüttemeister, S., & Klein U. 2001, *A&A*, 365, 571
- Weiss, A., Walter, F., Neininger, N., & Klein, U. 1999, *A&A*, 345, L23
- Wills, K. A., Redman, M. P., Muxlow, T. W. B., & Pedlar, A. 1999, *MNRAS*, 309, 395
- Young, J. S., Claussen, M. J., Kleinmann, S. G., Rubin, V. C., & Scoville, N. 1988, *ApJL*, 331, L81

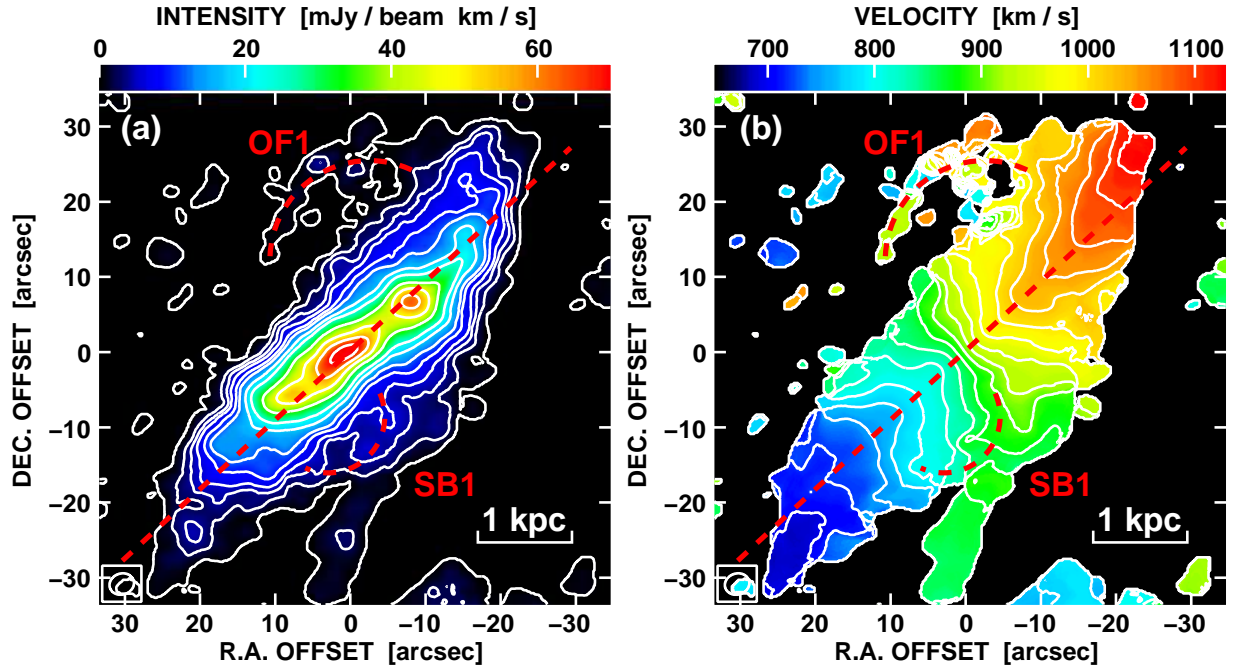


**Fig. 1.**  $^{12}\text{CO}(1-0)$  integrated intensity (moment 0) and intensity weighted mean velocity field (moment 1) maps of NGC 2146. The central position corresponds to R.A. =  $6^{\text{h}}18^{\text{m}}37^{\text{s}}.6$  and Dec. =  $78^{\circ}21'24''.1$  (J2000). The synthesized beam size is  $2''.8 \times 3''.4$ , which is shown at the bottom left corner of each figure. The red straight dashed lines indicate the position of the major axis (P.A. =  $137^{\circ}$ ). The *SB1* label indicates the position of an expanding superbubble, and the arc *OF1* shows an outflow, possibly a remnant of an expanding superbubble. The linear structure elongated from *SB1* toward the south is associated with a dust lane or “dust finger” (see Sect. 3 for details). (a)  $^{12}\text{CO}(1-0)$  moment 0 map. The contour levels are  $(0.1, 4, 7, 10, 15, 20, 30, 40, 60, 80, 100, \text{ and } 120) \times 585 \text{ mJy beam}^{-1} \text{ km s}^{-1}$  ( $= 5.69 \text{ K km s}^{-1}$ ). (b)  $^{12}\text{CO}(1-0)$  moment 1 map. The contour levels are from 695, 720, 745, ..., and 1120  $\text{km s}^{-1}$ , increasing with 25  $\text{km s}^{-1}$ .

**Table 1.** The properties of the two Molecular Superbubbles, *SB1* and *SB2*, and of the Outflow *OF1*

Component	Radius [pc]	Velocity [ $\text{km s}^{-1}$ ]	Timescale [ $10^7 \text{ yr}$ ]	Mass [ $10^8 M_{\odot}$ ]	Energy [ $10^{54} \text{ erg}$ ]
<i>SB1</i>	800 – 1200	$50 \pm 10$	1.3 – 2.9	2.6	4.1 – 9.3
<i>SB2</i>	400 – 1000	$35 \pm 10$	0.9 – 3.9	0.39	0.24 – 0.79
<i>OF1</i>	2000	0 – 200	1.0 – 2.0	3.4	30

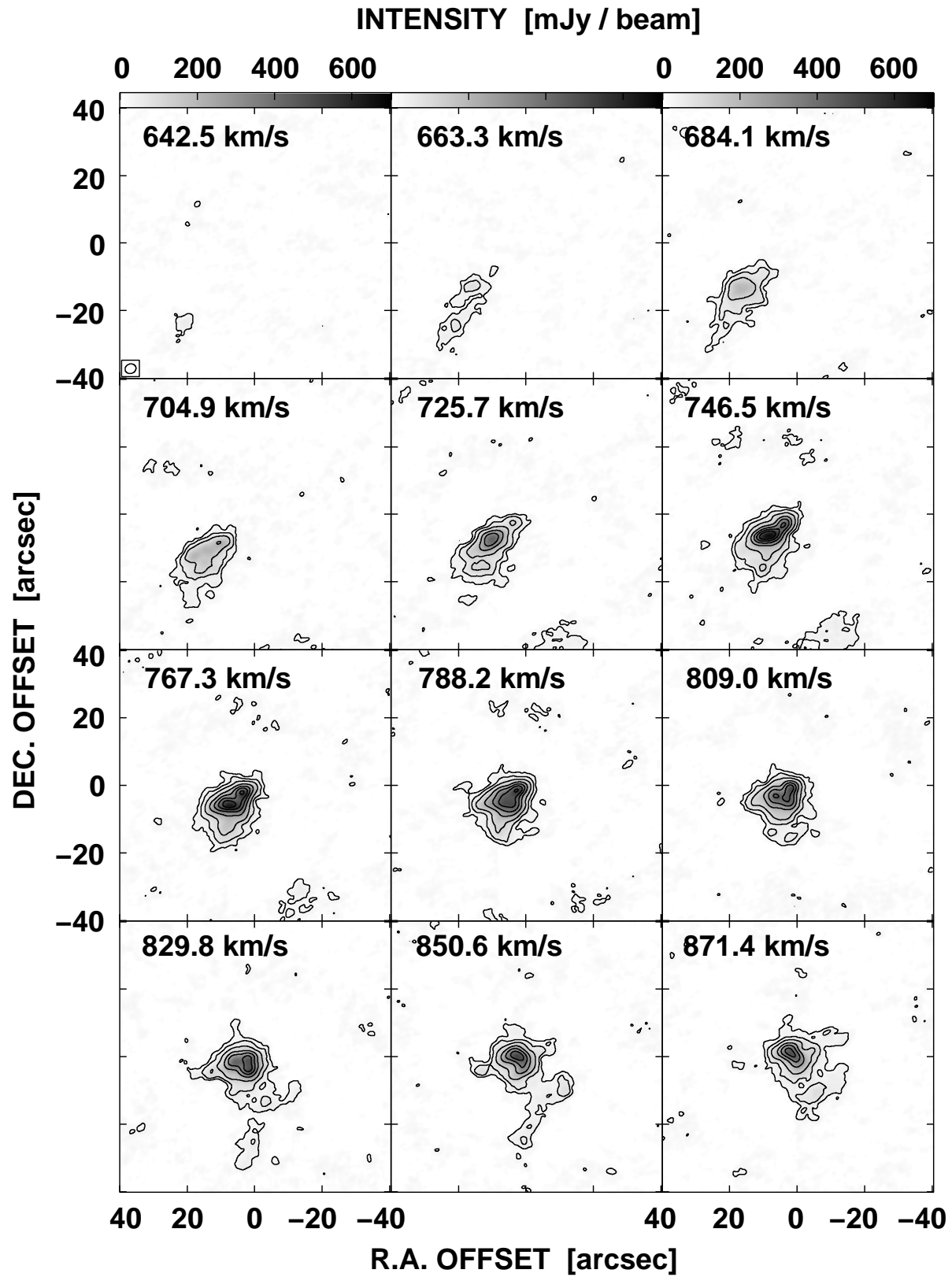


**Fig. 2.**  $^{12}\text{CO}(1-0)$  channel maps of NGC 2146. The central position and the synthesized beam size are the same as in figure 1, and the beam is shown in the lower left corner of panel 1. The contour levels are 5, 10, 20, 40, 60, 80, and  $100\sigma$ , where  $1\sigma$  is  $5.7 \text{ mJy beam}^{-1}$ . The LSR velocity is showing at the top left corner of each channel map.

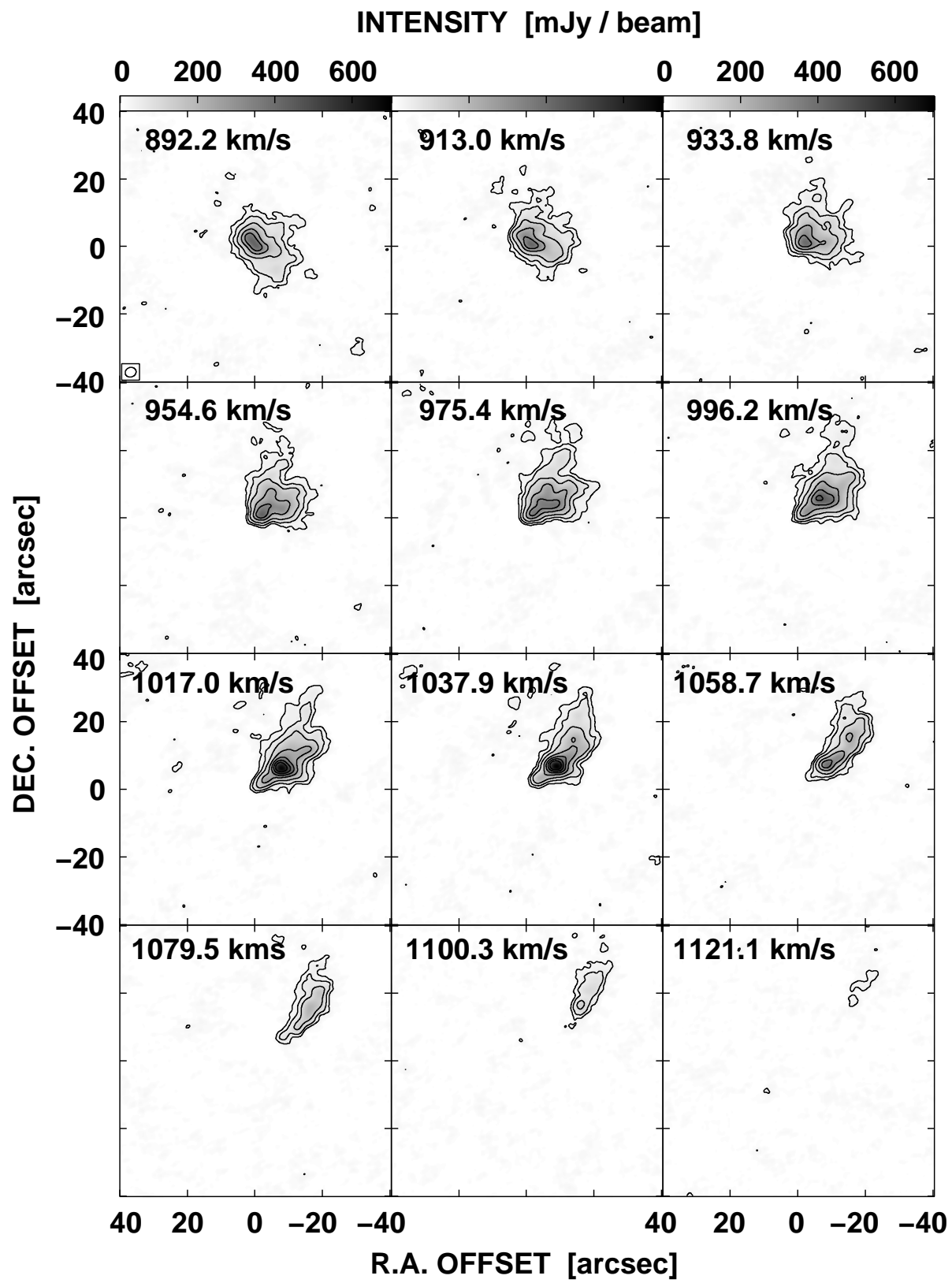
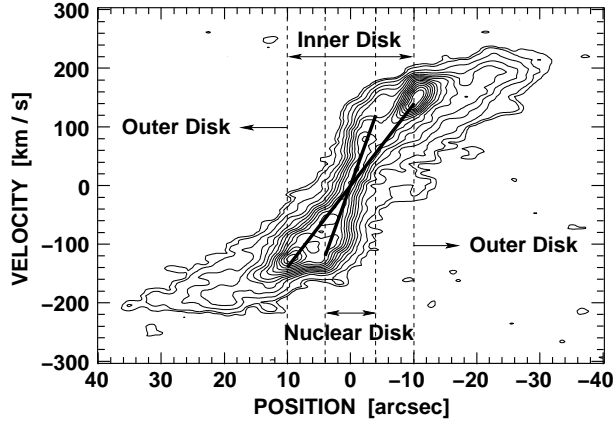
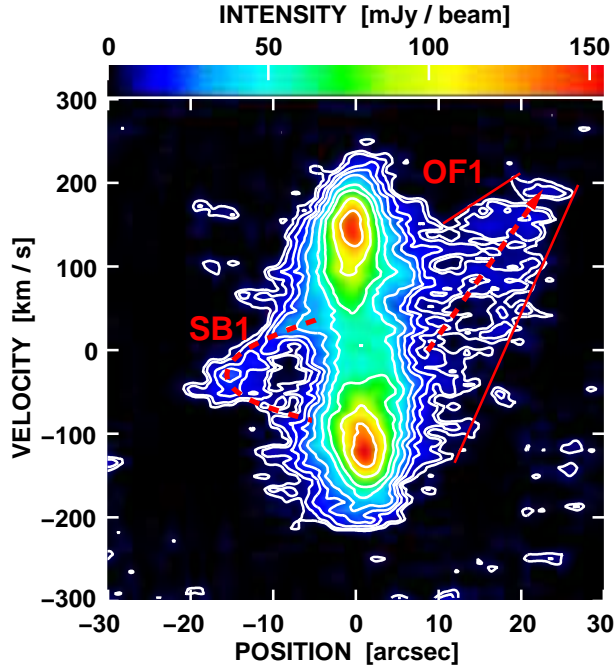


Fig. 2. Continued.



**Fig. 3.** The  $p-v$  diagram of NGC 2146 along the major axis. The central position corresponds to R.A. =  $6^{\text{h}}18^{\text{m}}37^{\text{s}}.6$ , and the central LSR velocity corresponds to  $900 \text{ km s}^{-1}$ . The contour levels are 3, 5, 10, 15, 20, ..., 65, and  $70\sigma$ , where  $1\sigma$  is  $0.01 \text{ Jy beam}^{-1}$ . The vertical dashed lines between  $\sim \pm 4''$  indicate the region of the nuclear disk, and those between  $\sim \pm 10''$  indicate the region of the inner disk, which are defined by the two rigid-rotating components shown in the thick solid lines. The outer regions, where kinematics are dominated by flat-rotation, are the outer disk.



**Fig. 4.** Major-axis-integrated  $p-v$  diagram along the minor axis. This  $p-v$  diagram is obtained by integrating the data along the major axis of the range between the position  $+22''$  and  $-28''$ , which is between two dotted vertical lines in figure 5. The position of zero corresponds to the major axis, and the zero velocity corresponds to the systemic velocity of  $900 \text{ km s}^{-1}$ . The contour levels are 2, 3, 5, 7, 10, 15, 20, 30, and  $40\sigma$ , where  $1\sigma$  is  $3.2 \text{ mJy beam}^{-1}$ . Here *SB1* and *OF1*, which are displayed in red dashed lines, indicate the positions of an expanding bubble and an outflow, which are shown in figure 1a (see section 3.2 for details). Two solid red lines indicate the range of the outflow.

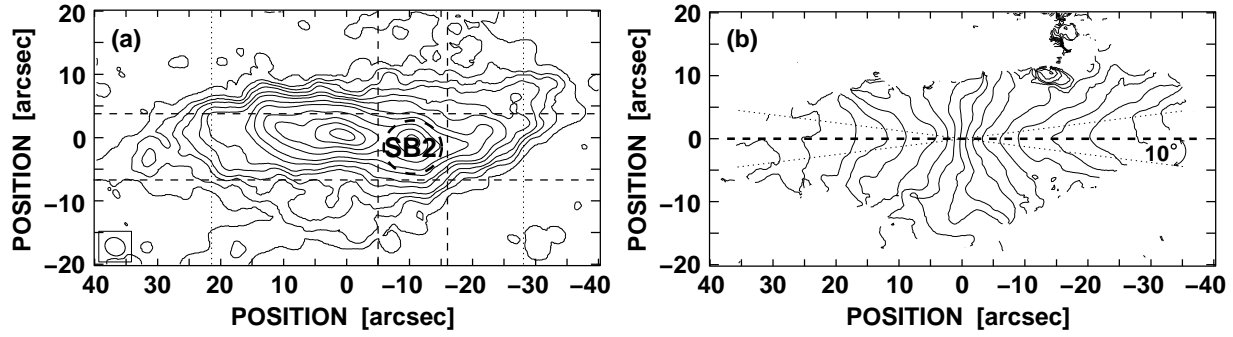


**Fig. 5.** (a) The integrated intensity map after a clockwise rotation of  $137^\circ$ . The contour levels are the same as in figure 1a. The two horizontal dashed lines, offset by  $-7''$  and  $+4''$  from the major axis, specify the range of major axis  $p-v$  diagrams shown in figure 6. The two vertical dashed lines,  $-5''$  and  $-16''$  from the minor axis, specify the range of the small molecular bubble *SB2*, and are the same as the two vertical dashed lines in figures 6 and 7. The thick dashed circle therefore indicates the region of *SB2*. The two vertical dotted lines indicate the integrated region of the  $p-v$  diagram in figure 4, which is between  $+22''$  and  $-28''$  along the minor axis. (b) The velocity field map after a clockwise rotation of  $137^\circ$ . The contour levels are the same as in figure 1b. The thick horizontal dashed line indicates the major axis. The two dotted lines specify the region (within  $\pm 10^\circ$  from the major axis) where the data points for the rotation curve shown in figure 8 were collected.



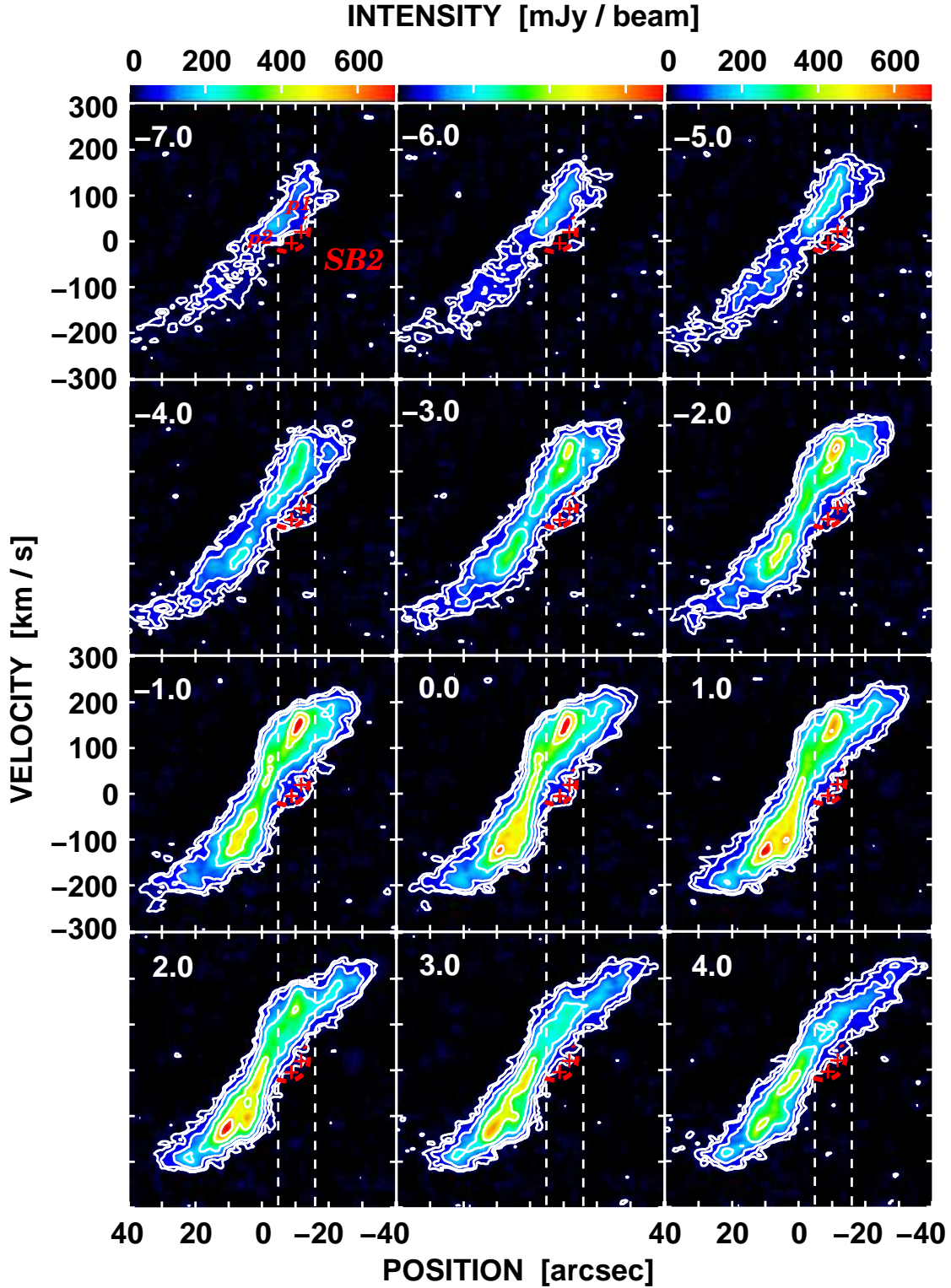


**Fig. 6.** The  $p-v$  diagrams along the major axis with various offsets. Each  $p-v$  diagram is averaged every  $2''$  with an interval of  $1''$ . The contour levels are  $3, 5, 10, 20, 40,$  and  $60\sigma$ , where  $1\sigma$  is  $10 \text{ mJy beam}^{-1}$ . The number in the top-left corner of each  $p-v$  diagram shows the position offset in units of arcseconds from the major axis in figure 5, which is offset by  $-7''$  to  $+4''$  from the major axis (see also figure 5). The red plus symbols,  $p1$  and  $p2$ , mark the possible centers of molecular bubbles. The velocity of the red plus symbols  $p1$  and  $p2$  are  $920$  and  $895 \text{ km s}^{-1}$ , respectively. The position of two vertical dashed lines are the same as in figure 5, namely,  $-5''$  and  $-16''$  offset from the minor axis.

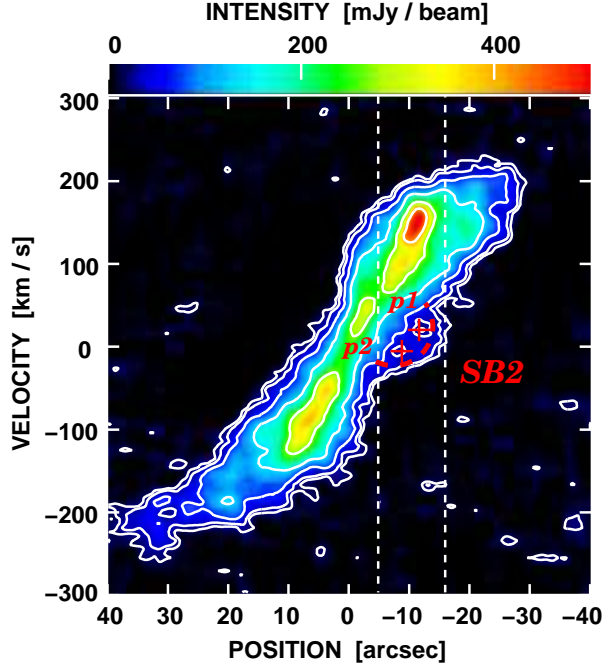


**Fig. 7.** The averaged  $p-v$  diagram of NGC 2146 and diffuse molecular bubbles  $SB2$ . The  $p-v$  diagram was made by averaging between  $-4''.8$  and  $0''.0$  offset from the major axis. The symbols  $p1$  and  $p2$  and the two vertical dashed lines are the same as in figure 6. The red dashed curve indicates the possible position of the molecular bubble  $SB2$ . The contour levels are 3, 5, 10, 20, 40, and  $60\sigma$ , where  $1\sigma$  is  $6.8 \text{ mJy beam}^{-1}$ .

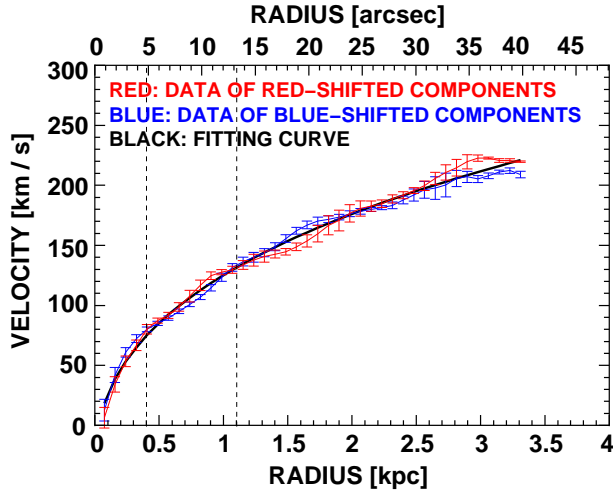


**Fig. 8.** Observed and fitted rotation curve along the major axis. The horizontal axis is the distance to the galactic center. The units in the lower axis are in kiloparsecs, and in the upper axis, arcseconds. The red and blue data are the redshifted and blueshifted components, respectively. The Elmegreen rotation curve is used for the fitting, and the black thick solid curve is the fitted rotation curve from both redshifted and blueshifted data. The vertical dashed lines in the radii of  $4''$  and  $10''$  indicate the sizes of the nuclear and the inner disks, respectively.

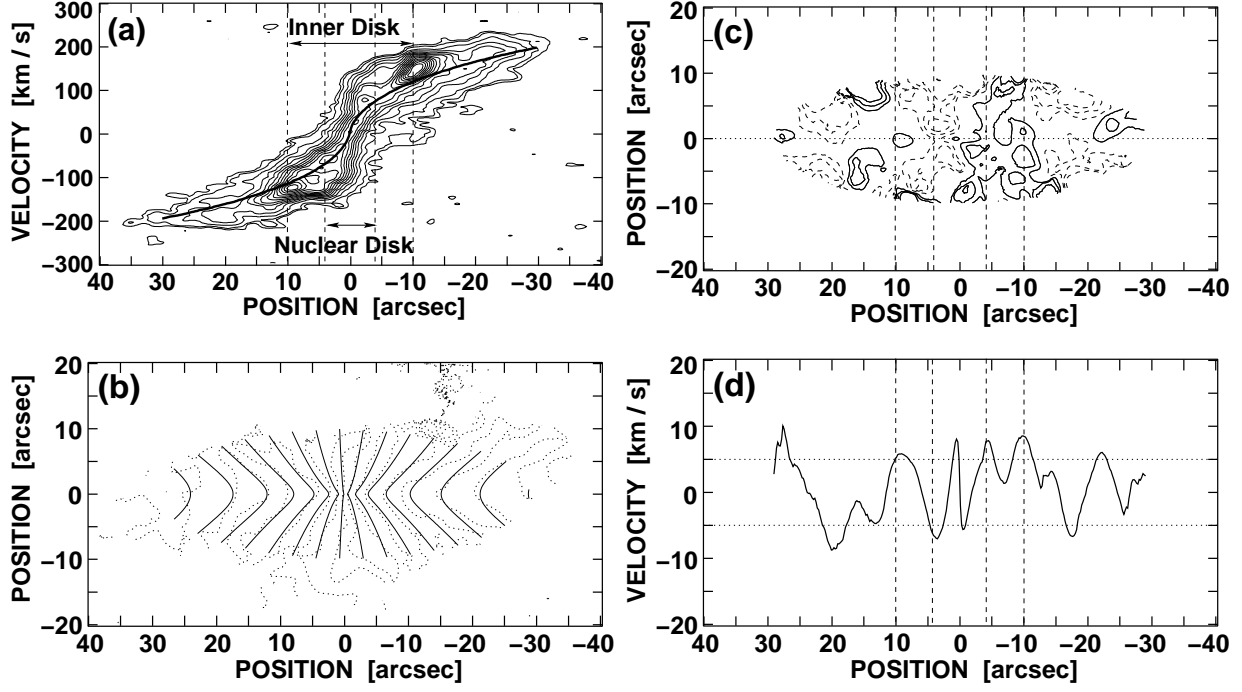
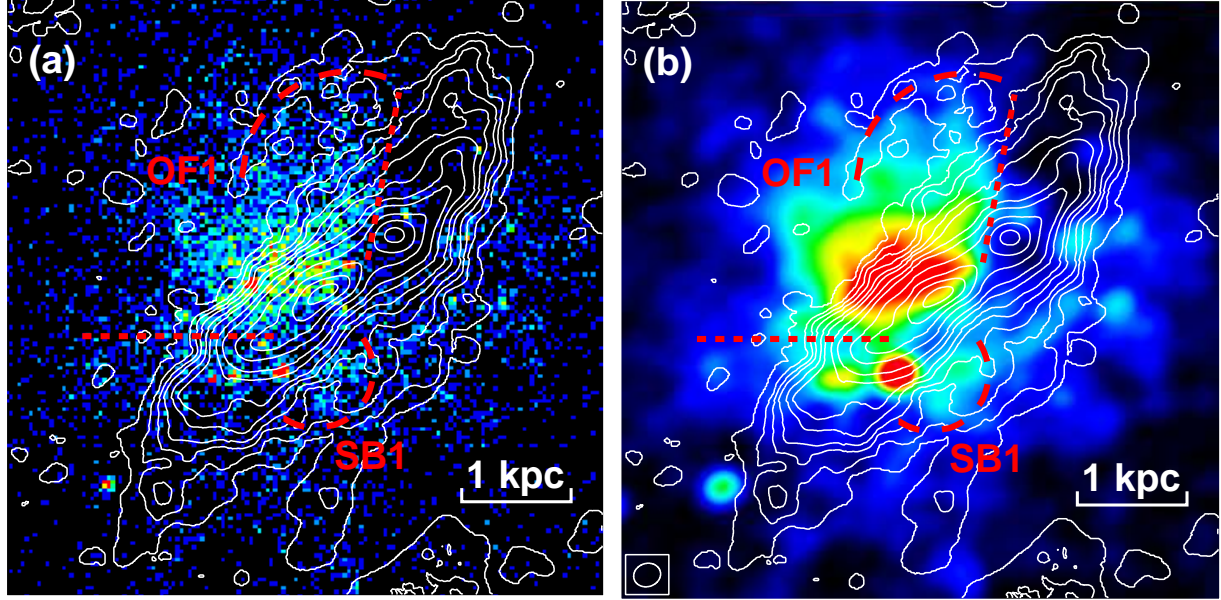
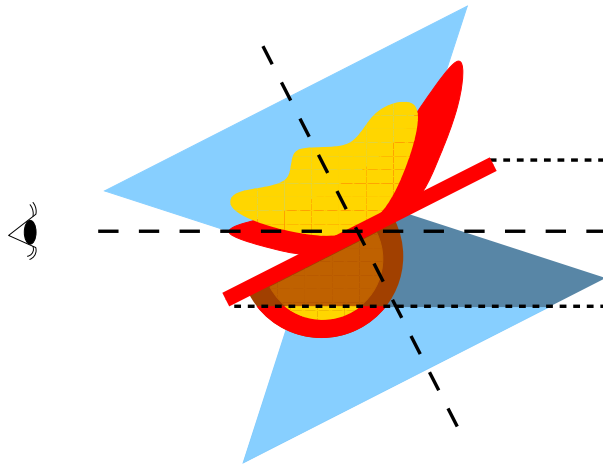


Fig. 9. (a) The  $p-v$  diagram with the fitted rotation curve. The contours are the  $p-v$  diagram along the major axis, which is the same as in figure 3. The black thick solid curve is the fitted rotation curve in figure 8. The vertical dashed lines show the range of the nuclear and inner disks. (b) A modeled velocity field map overlaid on the observed velocity map. The solid lines display the modeled velocity map, which is created from the fitted rotation curve in figure 9a. The contour levels, from left to right, are 720, 745, 770, ..., 1095  $\text{km s}^{-1}$ , increasing with 25  $\text{km s}^{-1}$ . The dotted lines are the velocity field map, which is the same as in figure 1b. (c) A residual velocity map. The residual velocity map is the differential values between the observed and the modeled velocity field maps. The solid contours are 5, 10, and 15  $\text{km s}^{-1}$ , and the dashed contours are -5, -10, and -15  $\text{km s}^{-1}$ . (d) A residual velocity along the major axis. The horizontal dotted lines indicates the velocity within  $\pm 5.2 \text{ km s}^{-1}$ , which is our velocity resolution. See Sect. 4 for more details.



**Fig. 10.** NMA  $^{12}\text{CO}(1-0)$  integrated intensity contour map overlaid on the Chandra soft X-ray image (Inui et al. 2005) in color-scale. The contour levels of the  $^{12}\text{CO}(1-0)$  map and the red long dashed lines marked as *SB1* and *OF1* are the same as in figure 1a. The X-ray outflow is collimated as shown between two red short dashed lines. Some weaker X-ray emission is concentrated inside *SB1*. (a) Without smoothing the soft X-ray image. (b) Smoothed to a beam size of  $2''.8 \times 3''.4$  (the same with that of the NMA image).



**Fig. 11.** The schematic diagram of outflows and superbubbles in NGC 2146 along the line-of-sight. The observer is on the left. The red colored region indicates the CO distribution, the yellow colored region indicates the soft X-ray emission distribution, and the blue colored region indicates optical emission line distribution. The gas behind the galactic disk is shaded to show it is absorbed by the galactic disk.